INTERNATIONAL JOURNAL FOR NUMERICAL AND ANALYTICAL METHODS IN GEOMECHANICS, VOL. 21, 721–737 (1997)

# ELASTOPLASTIC DEFORMATION AROUND UNDERGROUND OPENINGS UNDER BIAXIAL INITIAL STRESS FIELD

YUZO OBARA* AND KATSUHIKO SUGAWARA†

*Department of Civil Engineering, Kumamoto University, 2-39-1 Kurokami, Kumamoto, 860 Japan*

## SUMMARY

Estimation of elastoplastic deformation around an underground opening induced by the excavation of it, especially displacement and strain field in plastic region, is presented in this paper, as well as the formulation for calculating the displacement and strain in the plastic region around the underground opening by the coupled Boundary Element Method - Characteristics Method (BEM-CM). In this method, the non-associated flow rule is adopted to calculate the displacement and strain field in the plastic region, which is determined by the integration of the displacement along characteristics lines under the boundary condition of the elastic displacement on an elastoplastic interface analysed. It is shown that this method is one of the accurate and effective methods for estimating not only the shape and extent of the plastic region but also the state of the displacement and strain in the plastic region around the underground opening, comparing the theoretical solution with numerical results by this method for a circular opening under hydrostatic initial stress condition. Furthermore, this method is applied to rectangular and horse-shoe shaped openings and the characteristics of the strain field in the plastic region are discussed. © 1997 by John Wiley & Sons, Ltd.

Int. J. Numer. Anal. Meth. Geomech., Vol. 21, 721–737 (1997)
(No. of Figures: 10 No. of Tables: 0 No. of Refs: 10)

Key words: elastoplastic problem; non-associated flow rule; boundary element method; characteristics method

## INTRODUCTION

The shape and extent of plastic region, the states of stress, displacement and strain around underground openings induced by the excavation are governed by its stability. To estimate these, various numerical method for an elastoplastic boundary problem have been proposed. The most widely used method is the finite element method.[1] However, the subdivision of the finite elements is indispensable to analyse the location of an elastoplastic interface and the state of strain in the plastic region with a high accuracy. As the result shows, the large CPU time and physical memory of a computer are necessary to carry out numerical analyses.

To solve this problem, Aoki *et al.*,[2] Aoki and Sugawara,[3] Sugawara *et al.*[4,5] and Obara *et al.*[6,7] have suggested the coupled boundary element - characteristics method (BEM-CM) for two-dimensional elastoplastic boundary problem. The BEM-CM makes full use of the advantages of

*Correspondence to Y. Obara, Professor, Department of Civil Engineering, Kumamoto University, 2-39-1 Kurokami, Kumamoto, 860 Japan
†Professor

CCC 0363–9061/97/100721–17$17.50

*Received 2 May 1996*
*Revised 1 April 1997*

the BEM[8] and the CM[9] to solve the passive yielding problem. By means of the BEM-CM, the precise solution can be obtained using only less CPU time and physical memory of a computer. Then the displacement and strain field in the plastic region around underground openings can be examined in detail. In the suggested BEM-CM, however, since the associated flow rule is adopted to compute the displacement and strain in the plastic region by the CM, there was a trend that the displacement and strain are estimated more than actual values.

In the present paper, the non-associated flow rule is introduced into the BEM-CM to calculate the displacement and strain field in the plastic region around underground openings. It is shown that this method is one of the accurate and effective methods for estimating not only the shape and extent of the plastic region but also the states of the displacement and strain in the plastic region around underground opening, comparing the theoretical solution with numerical results for a circular opening under hydrostatic initial stress condition. Furthermore, this method is applied to rectangular and horse-shoe shaped opening and the characteristics of the displacement and strain field in the plastic region are discussed.

## OUTLINE OF BEM-CM

The formulation of the BEM-CM using the associated flow rule have been reported in detail, as well as the numerical procedure in References 2–7. In this chapter, the outline of the BEM-CM is described briefly.

In the BEM-CM, the analytical domain is divided into two regions, namely the elastic region $\Omega_1$ and the plastic region $\Omega_2$. The former is analysed by the BEM, and the latter is analysed by the CM. The boundary between $\Omega_1$ and $\Omega_2$ is incrementally modified and determined as the stress state on the boundary satisfies a chosen yield function.

Figure 1 is an example of the partial yielding of a single underground opening. The free surface of the opening consists of the elastic surface represented by $\Gamma_1$ and the plastic surface represented by $\Gamma_2$. The boundary between $\Omega_1$ and $\Omega_2$ is given by a curve represented by $\Gamma_3$, which is the so-called elastoplastic interface. The continuity of stress on the elastoplastic interface must be guaranteed everywhere on $\Gamma_3$, that is the normal stress and the shear stress on

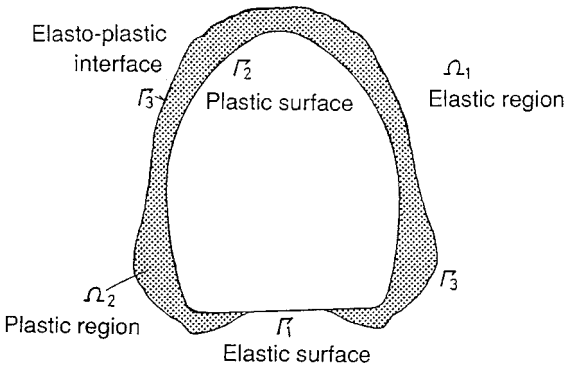


Figure 1. Partial yielding around an opening

 

$\Gamma_3$ are, respectively, the same on the both sides of $\Gamma_3$. The displacement needs to be continuous everywhere on $\Gamma_3$.

The present analysis is performed under the plane strain condition, and it is assumed that the rock is isotropic and homogeneous, and that the stress in the plastic region always satisfies a chosen yield function: $f(\sigma_{ij}) = 0$. Therefore, the stress $\sigma^{e}_{ij}$ in $\Omega_1$ are conditioned by $f(\sigma^{e}_{ij}) < 0$, and the stress $\sigma^{p}_{ij}$ in $\Omega_2$ by $f(\sigma^{p}_{ij}) = 0$.

The elastoplastic interface is determined by an iteration, that is the step-by-step widening of the plastic region. In the iteration, the CM is used to solve the equilibrium equations within the plastic region and to determine the traction acting on the elastoplastic interface, and the BEM is used to compute the stresses within the elastic region.

Prior to the iteration, the elastic-stress analysis is performed by the BEM, assuming an isotropic homogeneous linear elasticity in the full analytical domain. Then, from analysed stress distribution on the free surface of the opening, the elastic surface $\Gamma_1$ is approximately assessed in the range of $f(\sigma^{e}_{ij}) < 0$, and the plastic surface $\Gamma_2$ in the range of $f(\sigma^{e}_{ij}) \geqslant 0$. The slip-line analysis by the CM is independently performed to determine the stress $\sigma^{p}_{ij}$ around the opening, corresponding to the stress condition on the free surface of the opening, and to assess the potential plastic region on the base of $\Gamma_2$. The curvilinear ABC in Figure 2 is an example of the potential plastic region.

In the iteration, the elastoplastic interface needs to be assigned, as $\Gamma_3$ in Figure 2, within the potential plastic region, then $\Gamma_2$ and $\Gamma_3$ have to be modified incrementally. The elastic region to be analysed by the BEM is, therefore, defined by $\Gamma_1$ and $\Gamma_3$, and the necessary boundary stress condition on $\Gamma_3$ is defined from the slip-line analysis previously mentioned.

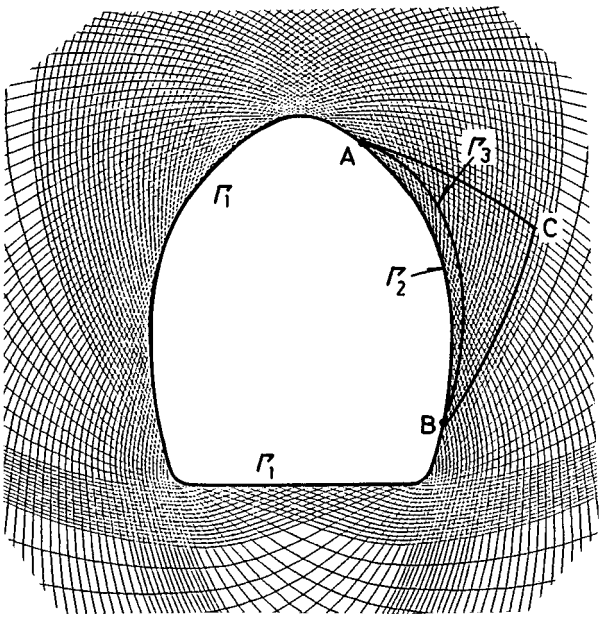


Figure 2. Passive slip line around an opening and a curvilinear triangle ABC on the base $\Gamma_2$

 

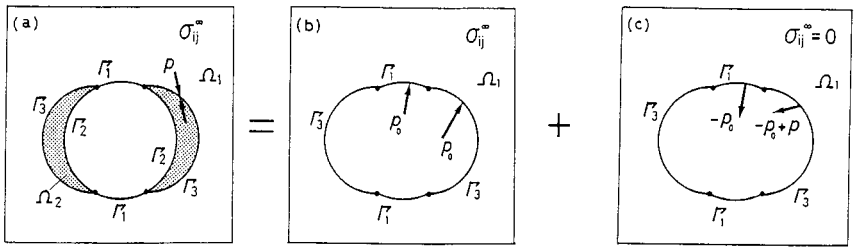


Figure 3. Principle of the superposition; (a) partial yielding of a circular opening, (b) initial stress field, (c) stress change in elastic region

The principle of the superposition, as illustrated in Figure 3, is available for the analysis of the stress $\sigma_{ij}^{e}$ in $\Omega_1$ by the BEM. The state (a) in Figure 3 represents an elastoplastic solution to be solved, that is, a partial yielding of bilateral symmetry around a circular opening, being subjected to the initial stress $\sigma_{ij}^{\infty}$ at infinity. The traction on $\Gamma_3$ is represented by $p$. The state (b) shows the initial state of the elastic region, being subjected to the initial stress $\sigma_{ij}^{\infty}$ at infinity. The traction $p_0$ on $\Gamma_1$ and $\Gamma_3$ is equivalent to $\sigma_{ij}^{\infty}$. The state (c) shows the stress changes in the elastic region. The stress field within the elastic region of the state (a) is obtained by superimposing the state (c) on state (b). Additionally, in the case that the traction $p$ is calculated from the stress $\sigma_{ij}^{p}$ by the Cauchy's formula, the condition of the stress continuity is always satisfied everywhere on $\Gamma_3$.

By examining the stress $\sigma_{ij}^{e}$ on $\Gamma_1$ and $\Gamma_3$, if there is a range of $f(\sigma_{ij}^{e}) \geqslant 0$ on $\Gamma_1$, it is added to $\Gamma_2$, and if there is a range of $f(\sigma_{ij}^{e}) \geqslant 0$ on $\Gamma_3$, the elastoplastic interface is translated outwards and, subsequently, the plastic region slightly expands. Such a step-by-step widening of the plastic region and the repitition of the stress analysis by the BEM is continued until the stress $\sigma_{ij}^{e}$ on $\Gamma_3$ satisfies the condition of $f(\sigma_{ij}^{e}) = 0$. This is the fundamental concept of the present method to determine the plastic region and the stress field.

The analysis of the displacement and strain field are subsequently performed. The CM is also available for this analysis. At that time, the boundary condition is given on the elastoplastic interface. This is the displacement on $\Gamma_3$ calculated by the BEM. In addition, it can be noted that the hardening and softening effect of a material can be easily incorporated in the BEM-CM, since the yield functions used in the plastic region and on the elastoplastic interface can be independently introduced.

## DISPLACEMENT IN PLASTIC REGION

In this method, Mohr–Coulomb's yield function is adopted to determine the stress field around underground opening, which is expressed as

$$f = \tau - C - \sigma \tan \phi \tag{1}$$

where $\tau$ and $\sigma$ are the shear and the normal stress, respectively, and $C$ and $\phi$ are the cohesion and the internal friction angle, respectively. On the other hand, the plastic potential which is different from the yield function is introduced to calculate displacement field in the plastic region, namely the non-associated flow rule, is used in this method. The plastic potential which is of the same

 

type as the yield function is defined at a plastic stress state as

$$g = \tau - C_{\mathrm{p}} - \sigma \tan \phi_N \tag{2}$$

where $C_{\mathrm{p}}$ is a constant dependent on the plastic stress state and $\phi_N$ is the dilatancy angle. Equations (1) and (2) are rewritten in terms of the principal stresses $\sigma_1$ and $\sigma_3$ ($\sigma_1 > \sigma_3 > 0$, the compressive stress is defined by possitive) as

$$f = (\sigma_1 - \sigma_3) - 2C \cos \phi - (\sigma_1 + \sigma_3) \sin \phi \tag{3}$$

$$g = (\sigma_1 - \sigma_3) - 2C_{\mathrm{p}} \cos \phi_N - (\sigma_1 + \sigma_3) \sin \phi_N \tag{4}$$

Now the plastic potential is assumed by using the stress components $\sigma_x$, $\sigma_y$ and $\tau_{xy}$ in the $x$–$y$ co-ordinates as

$$g = \sqrt{(\sigma_x - \sigma_y)^2 + \tau_{xy}^2} - 2C_{\mathrm{p}} \cos \phi - (\sigma_x + \sigma_y) \sin \phi_N \tag{5}$$

The non-associated flow rule is defined in terms of the plastic potential expressed as

$$d\{\varepsilon^{\mathrm{p}}\} = \lambda^* \frac{\partial g}{\partial \{\sigma\}} \tag{6}$$

where $\lambda^*$ is a constant, $\{\ \}$ represents vector and the superscript p refers to the plastic strain. The plastic strain components are defined as

$$\begin{aligned} \mathrm{d}\varepsilon_x^{\mathrm{p}} &= \lambda^* \frac{\partial g}{\partial \sigma_x} = \lambda \left( \frac{\sigma_x - \sigma_y}{2T} - \sin \phi_N \right) \\ \mathrm{d}\varepsilon_y^{\mathrm{p}} &= \lambda^* \frac{\partial g}{\partial \sigma_y} = \lambda \left( \frac{\sigma_y - \sigma_x}{2T} - \sin \phi_N \right) \\ \mathrm{d}\gamma_{xy}^{\mathrm{p}} &= \lambda^* \frac{\partial g}{\partial \tau_{xy}} = \lambda \left( \frac{\tau_{xy}}{T} \right) \end{aligned} \tag{7}$$

where

$$T^2 = \frac{(\sigma_x - \sigma_y)^2}{4} + \tau_{xy}^2 = \frac{(\sigma_1 - \sigma_3)^2}{4} \tag{8}$$

Designating the inclination of $\sigma_1$ from the $x$-axis by $\beta$ as shown in Figure 4(a), the stress components in the $x$–$y$ co-ordinates, within the plastic region, are expressed as

$$\begin{aligned} \sigma_x &= \frac{\sigma_1 + \sigma_3}{2} + \frac{\sigma_1 - \sigma_3}{2} \cos 2\beta \\ \sigma_y &= \frac{\sigma_1 + \sigma_3}{2} - \frac{\sigma_1 - \sigma_3}{2} \cos 2\beta \\ \tau_{xy} &= \frac{\sigma_1 - \sigma_3}{2} \sin 2\beta \end{aligned} \tag{9}$$

and

$$\sigma_x - \sigma_y = (\sigma_1 - \sigma_3) \cos 2\beta = 2T \cos 2\beta \tag{10}$$

 

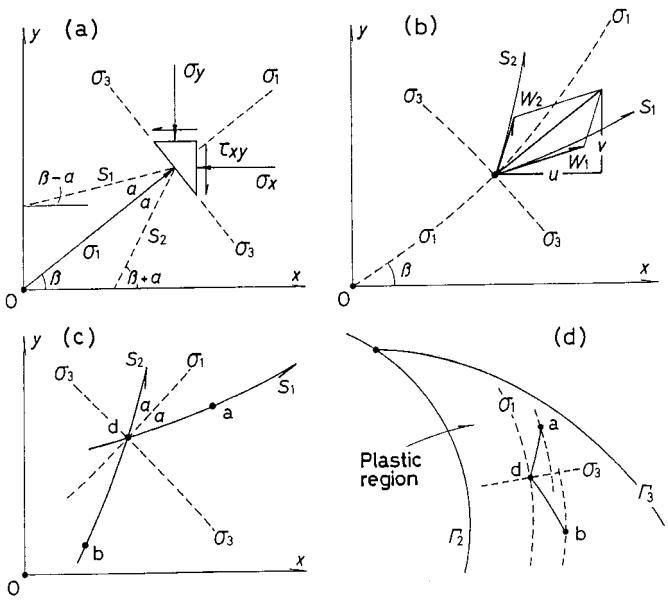


Figure 4. Method of characteristics for displacement analysis in plastic region; (a) co-ordinates and stress components, (b) displacement along slip lines, (c) slip lines, $S_1$ and $S_2$, and nodal points, (d) displacement analysis based on the continuity of displacement on $\Gamma_3$

Substituting equation (9) into equation (7), we obtain the following:

$$\begin{aligned} \mathrm{d}\varepsilon_x^{\mathrm{p}} &= \lambda(\cos 2\beta - \sin \phi_N) \\ \mathrm{d}\varepsilon_y^{\mathrm{p}} &= -\lambda(\cos 2\beta + \sin \phi_N) \\ \mathrm{d}\gamma_{xy}^{\mathrm{p}} &= \lambda \sin 2\beta \end{aligned} \tag{11}$$

Then, the principal plastic strains are given as

$$\begin{aligned} \mathrm{d}\varepsilon_1^{\mathrm{p}} &= \lambda(1 - \sin \phi_N) \\ \mathrm{d}\varepsilon_3^{\mathrm{p}} &= -\lambda(1 + \sin \phi_N) \end{aligned} \tag{12}$$

Therefore, the constant $\lambda$ in the following equation is

$$\lambda = \frac{\mathrm{d}\varepsilon_1^{\mathrm{p}} - \mathrm{d}\varepsilon_3^{\mathrm{p}}}{2} \tag{13}$$

By eliminating the constant $\lambda$ in equation (11), we obtain the following:

$$\begin{aligned} \mathrm{d}\varepsilon_x^{\mathrm{p}} - \mathrm{d}\varepsilon_y^{\mathrm{p}} &= 2\mathrm{d}\gamma_{xy}^{\mathrm{p}} \cot 2\beta \\ \mathrm{d}\varepsilon_x^{\mathrm{p}} + \mathrm{d}\varepsilon_y^{\mathrm{p}} &= -2\mathrm{d}\gamma_{xy}^{\mathrm{p}} \frac{\sin \phi_N}{\sin 2\beta} \end{aligned} \tag{14}$$

 

Then equation (14) is integrated as follows, by assuming the angle $\beta$ to be constant at a certain location in the plastic region

$$\begin{aligned} \varepsilon_x^{\mathrm{p}} - \varepsilon_y^{\mathrm{p}} &= 2\gamma_{xy}^{\mathrm{p}} \cot 2\beta \\ \varepsilon_x^{\mathrm{p}} + \varepsilon_y^{\mathrm{p}} &= -2\gamma_{xy}^{\mathrm{p}} \frac{\sin \phi_N}{\sin 2\beta} \end{aligned} \tag{15}$$

On the other hand, the displacement components, $u$ and $v$ are defined in the $x$–$y$ co-ordinates in Figure 4(b), expressed as

$$u = u_0 + \Delta u, \quad v = v_0 + \Delta v \tag{16}$$

where $u_0$ and $v_0$ are the initial displacement components and $\Delta u$ and $\Delta v$ are the displacement due to excavation. Under the initial stress condition, the initial displacement components are given as

$$\begin{aligned} 2Gu_0 &= \{(1-\nu)\sigma_x - \nu\sigma_y\} x + \tau_{xy} y \\ 2Gv_0 &= \{-\nu\sigma_x + (1-\nu)\sigma_y\} y + \tau_{xy} x \end{aligned} \tag{17}$$

where $G$ and $\nu$ are the shear modulus and the Poisson's ratio, respectively.

The total strain in the plastic region can be obtained as the sum of the elastic strain and the plastic strain, and the strain components are defined by the following equations:

$$\begin{aligned} \varepsilon_x &= \varepsilon_x^{\mathrm{e}} + \varepsilon_x^{\mathrm{p}} = \frac{\partial u}{\partial x} \\ \varepsilon_y &= \varepsilon_y^{\mathrm{e}} + \varepsilon_y^{\mathrm{p}} = \frac{\partial v}{\partial y} \\ \gamma_{xy} &= \gamma_{xy}^{\mathrm{e}} + \gamma_{xy}^{\mathrm{p}} = \frac{1}{2}\left(\frac{\partial u}{\partial y} + \frac{\partial v}{\partial x}\right) \end{aligned} \tag{18}$$

where the superscript e refers to the elastic component. From the elastic stress–strain relation under the plane strain condition, the elastic strain components are given as follows:

$$\begin{aligned} 2G\varepsilon_x^{\mathrm{e}} &= (1-\nu)\sigma_x - \nu\sigma_y \\ 2G\varepsilon_y^{\mathrm{e}} &= -\nu\sigma_x + (1-\nu)\sigma_y \\ 2G\gamma_{xy}^{\mathrm{e}} &= \tau_{xy} \end{aligned} \tag{19}$$

By substituting equations (18) into equations (15), we obtain

$$\begin{aligned} \frac{\partial u}{\partial x} - \cos 2\beta \frac{\partial u}{\partial y} - \cos 2\beta \frac{\partial v}{\partial x} - \frac{\partial u}{\partial y} &= 0 \\ \frac{\partial u}{\partial x} + \frac{\sin \phi_N}{\sin 2\beta}\frac{\partial u}{\partial y} + \frac{\sin \phi_N}{\sin 2\beta}\frac{\partial v}{\partial x} + \frac{\partial u}{\partial y} &= h \end{aligned} \tag{20}$$

 

where

$$h = \varepsilon_x^e + \varepsilon_y^e + 2\gamma_{xy}^e \frac{\sin\phi_N}{\sin 2\beta} \tag{21}$$

Equations (20) are the hyperbolic-type partial differential equations for $u$ and $v$, and the characteristics curves coincide with the slip lines $S_1$ and $S_2$ in Figure 4(c), expressed as

$$\frac{dy}{dx} = \tan(\beta \pm \alpha), \quad \alpha = \frac{\pi}{4} - \frac{\phi_N}{2} \tag{22}$$

Since $S_1$ and $S_2$ intersect each other at angles $\beta - \alpha$ and $\beta + \alpha$, respectively, the derivatives of the slip line are expressed as

$$\begin{aligned} \cos\phi_N \frac{\partial}{\partial x} &= \sin(\beta + \alpha)\frac{d}{dS_1} - \sin(\beta - \alpha)\frac{d}{dS_2} \\ \cos\phi_N \frac{\partial}{\partial y} &= -\cos(\beta + \alpha)\frac{d}{dS_1} + \cos(\beta - \alpha)\frac{d}{dS_2} \end{aligned} \tag{23}$$

and the displacement components the $x$–$y$ co-ordinates are represented by the displacement components $W_1$ and $W_2$ along the slip lines $S_1$ and $S_2$ as shown in Figure 4(b)

$$\begin{aligned} u &= W_1\cos(\beta - \alpha) + W_2\cos(\beta + \alpha) \\ v &= W_1\sin(\beta - \alpha) + W_2\sin(\beta + \alpha) \end{aligned} \tag{24}$$

By making use of equations (24) and the partial derivatives of equations (23), equations (20) can be rewritten as two differential equations expressing the two variables of $W_1$ and $W_2$ along the slip lines.

$$\begin{aligned} \frac{dW_1}{dS_1} + \sin\phi_N \frac{dW_2}{dS_1} - W_2\cos\phi_N \frac{d\beta}{dS_1} &= \frac{h}{2} \\ \frac{dW_2}{dS_2} + \sin\phi_N \frac{dW_1}{dS_2} + W_1\cos\phi_N \frac{d\beta}{dS_2} &= \frac{h}{2} \end{aligned} \tag{25}$$

If the segments, $\overline{ad}$ and $\overline{db}$, of two intersecting slip lines are defined as shown in Figure 4(c), equations (25) may be replaced by the linear differential equations for $W_1$ and $W_2$, that is

$$\begin{aligned} W_{1a} - W_{1d} + \sin\phi_N(W_{2a} - W_{2d}) - \cos\phi_N \frac{W_{2a} + W_{2d}}{2}(\beta_a - \beta_d) &= \frac{h_a - h_d}{4}\overline{ad} \\ W_{2d} - W_{2b} + \sin\phi_N(W_{1d} - W_{1b}) + \cos\phi_N \frac{W_{1d} + W_{1b}}{2}(\beta_d - \beta_b) &= \frac{h_d - h_b}{4}\overline{bd} \end{aligned} \tag{26}$$

where $\overline{ad}$ and $\overline{bd}$ imply the distance between the nodal points. $W_{1a}$ means the displacement $W_1$ at the nodal point a. The first approximation of $W_{1d}$ and $W_{2d}$ is obtained by solving equations (26) and may be corrected by the step-by-step method.

 

## NUMERICAL EXAMPLES

*A circular opening*

To demonstrate the accuracy of the solution by the BEM-CM, the method is applied to the circular opening of the radius $R$ under a hydrostatic initial stress condition, namely $\sigma_x^\infty = \sigma_y^\infty = \sigma_0^\infty$, $n = \sigma_0^\infty / S_c$, where $S_c$ is the uniaxial compressive strength. The shear modulus $G$ and the Poisson's ratio $v$ of rock mass are 1·7 GPa and 0·2, respectively. In the analysis, the dilatancy angle is changed.

According to theory,[10] the plastic region is formed as a ring under the hydrostatic initial stress condition. In this case, the radius of the elastoplastic interface $R^*$ is given as follows:

$$\left(\frac{R^*}{R}\right)^{q-1} = \frac{2\{(q-1)n+1)\}}{q+1} \tag{27}$$

On the other hand, the total displacement $u_r$ in the radial direction is written as follows (see appendix):

$$\begin{aligned} 2G\frac{u_r}{r} = {} & \frac{S_c}{1-q}\left\{(1-2v) - \frac{(1-v)(qq_N+1) - v(q+q_N)}{q+q_N}\right\}\left(\frac{r}{R}\right)^{q-1} \\ & + \frac{2(1-v)}{q+q_N}\{(q-1)\sigma_0^\infty + S_c\}\left(\frac{R^*}{r}\right)^{q+1} \end{aligned} \tag{28}$$

where $S_c = 2C\tan\left(\frac{\pi}{4}+\frac{\phi}{2}\right)$, $q = \tan^2\left(\frac{\pi}{4}+\frac{\phi}{2}\right)$ and $q_N = \tan^2\left(\frac{\pi}{4}+\frac{\phi_N}{2}\right)$.

Figure 5 shows the comparison of the numerical results with the theoretical solutions (Appendix). In this figure, the lateral axis is the distance from the opening wall and the longitudinal axis is the normalized displacement $u_r$. The black circles are numerical results and the solid lines are the theoretical solutions. The radius of the elastoplastic interface is 1·148$R$ and coincides with the theoretical value calculated by equation (27). The numerical distribution of the displacement in the plastic region is in good agreement with the analytical one in the case of adopting the associated flow rule. On the other hand, the difference of both becomes greater with increasing the difference between the internal friction angle $\phi$ and the dilatancy angle $\phi_N$. Because of which the integration pass of calculating displacement is not the same that of calculating stress in the plastic region in the case of adopting non-associated flow rule. However, the maximum error of the displacement on the opening wall is about 1% in the case of $\phi_N = 0^\circ$. Therefore, the proposed method is available for evaluating the deformation around the opening. It is noted that the degree of the deformation decreases with the reduction of $\phi_N$.

From this comparison, it is concluded that the BEM-CM is an accurate and effective method for estimating not only the shape and extent of the plastic region but also the states of the displacement and strain in the plastic region around underground opening.

*Rectangular openings*

To examine the characteristics of the displacement and strain in the plastic region around the opening, the suggested method is applied to rectangular openings, having a different radius of

 

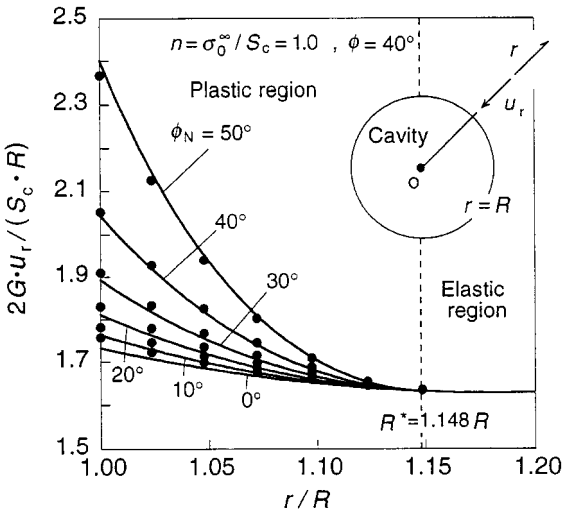


Figure 5. Comparison of numerical results with the theoretical solutions concerning the location of elastoplastic interface and the distribution of displacement around a circular opening in the case of using the non-associated flow rule

curvature at corners. The geometry of the openings as shown in Figure 6 is $H_y$ in height and $H_x$ in width. The radiuses $r_0$ of curvature at the corner of two openings are $r_0/H_y = 0{\cdot}026$ in Case 1 and 0·15 in Case 2, respectively. The analytical condition is described in the figure. Figure 7 shows the displacement of the opening surface in the case of adopting the associated flow rule and Figure 8 is for the case of adopting the non-associated flow rule, $\phi \neq \phi_N = 0°$. The state of elastoplastic displacement of the opening surface is compared with that of elastic displacement in these figures. $\Delta u$ in the figures represents the displacement due to excavation. The slip lines are drawn in the plastic region around the openings.

The place of which the depth of the plastic region in both cases is largest is located at the centre of both side walls. Its depth in Case 2 is 85 per cent of that in Case 1. The depth of the roof and floor in Case 2 is 72 per cent of that in Case 1. It is also found that the depth of the corner in Case 2 is smaller than that in Case 1. In the case of using the associated flow rule as shown in Figure 7, the elastic displacement of the opening surface maximizes at the centre of the side wall. The elastoplastic displacement of it is small at the corner and uniform throughout the wall. The value of the displacement of the roof and floor in Case 2 is 88 per cent of that in Case 1. It is confirmed that the shape of the rectangular opening having a larger radius of curvature at the corner has a mechanical advantage to decrease the depth of the plastic region and the displacement.

On the other hand, in the case of using the non-associated flow rule as shown in Figure 8, the extent and shape of the plastic region coincide with those in Figure 7. Because of which the excavation of the openings is assumed as whole excavation and that the stress and the displacement field around opening are calculated independently in this analysis. Therefore, to simulate actual excavation of the opening, an incremental method is necessary to be adopted in the analysis. The elastoplastic displacement decreases, comparing with that in Figure 7. The deformed shape of the surface of the elastoplastic solution is almost the same as that of the elastic

 

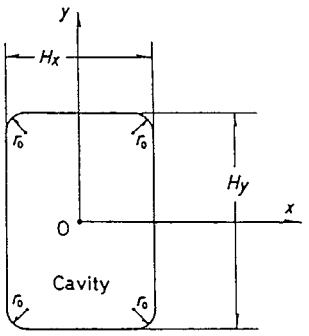


Analytical condition; $\sigma_x^\infty = \sigma_y^\infty = \sigma_0^\infty$ , $n = \sigma_0^\infty / S_c = 1.8$,
$S_c(H_y/2)/2G = 0.6238$, $\nu = 0.2$, $\phi = 40°$,
case 1 : $r_0/H_y = 0.026$, case 2 : $r_0/H_y = 0.15$

Figure 6. A rectangular opening and the co-ordinates

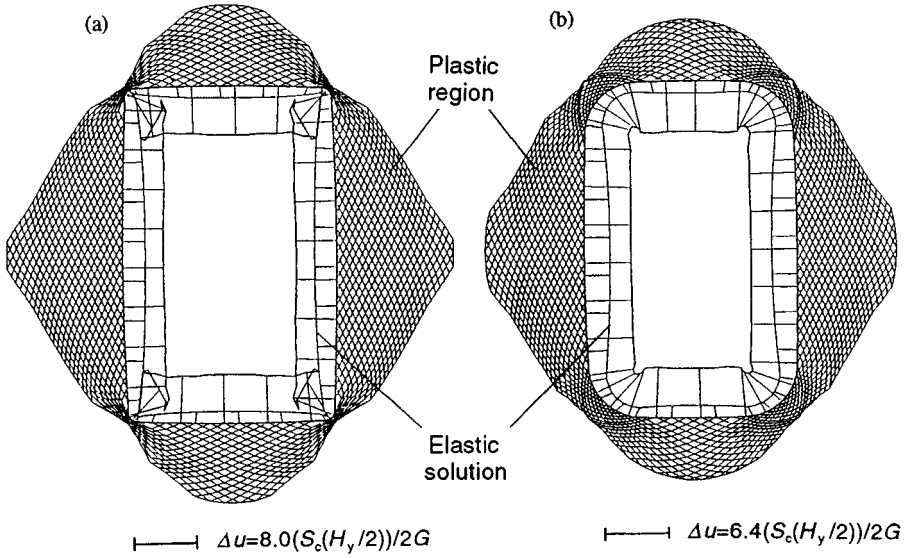


Figure 7. Shape and extent of the plastic region, and displacement of the opening wall in the case of using associated flow rule, dilatancy angle $\phi_N = 40°$ (the slip lines corresponding to the boundary element divided on the elastoplastic interface are drawn in the plastic region); (a) Case 1, (b) Case 2

solution. It is concluded that the non-dilatant rock mass behaves as the elastic rock mass having the smaller elastic moduli than the original ones.

The principal plastic strains is defined by $\varepsilon_1^p$ and $\varepsilon_3^p$. The volumetric plastic strain $(\varepsilon_1^p + \varepsilon_3^p)$ is proportional to the maximum plastic shear strain $(\varepsilon_1^p - \varepsilon_3^p)/2$ as follows:

$$\varepsilon_1^p + \varepsilon_3^p = -(\varepsilon_1^p - \varepsilon_3^p)\sin\phi_N \tag{29}$$

Accordingly, the dilatancy is proportional to the differential plastic strain $(\varepsilon_1^p - \varepsilon_3^p)$. In the analysis, the maximum total shear strain $(\varepsilon_1 - \varepsilon_3)/2$ and the maximum elastic shear strain

 

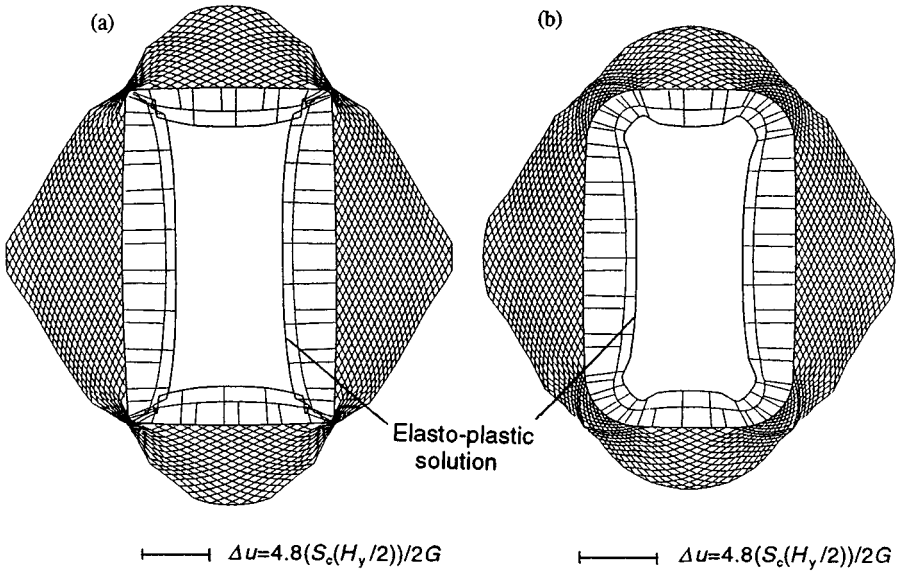


Figure 8. Shape and extent of the plastic region, and displacement of the opening wall in the case of using non-associated flow rule, dilatancy angle $\phi_N = 40°$; (a) Case 1, (b) Case 2

$(\varepsilon_1^e - \varepsilon_1^e)/2$ are calculated at the intersection of slip lines as follows:

$$\frac{(\varepsilon_1 - \varepsilon_3)}{2} = -\frac{1}{2}\left(\frac{\partial W_1}{\partial S_2} + \frac{\partial W_2}{\partial S_1}\right)$$
$$\frac{(\varepsilon_1^e - \varepsilon_3^e)}{2} = \frac{(1+\nu)(\sigma_1 - \sigma_3)}{2E} \tag{30}$$

Consequently, the maximum plastic shear strain can be obtained as follows:

$$\frac{(\varepsilon_1^p - \varepsilon_3^p)}{2} = \frac{(\varepsilon_1 - \varepsilon_3)}{2} - \frac{(\varepsilon_1^e - \varepsilon_3^e)}{2} \tag{31}$$

Figure 9 shows the contour map of $(\varepsilon_1^p - \varepsilon_3^p)$ in the plastic region in the case of $\phi = \phi_N = 40°$. The maximum plastic shear strain is induced at the corner of the opening in both cases. The values of those are $380 \times 10^{-3}$ in Case 1 and $65 \times 10^{-3}$ in Case 2, respectively. The value in Case 1 is about six times as large as that in Case 2. The concentration of the contour lines appears near the corner of the opening in both cases. In Case 1, the interval of the contour lines is narrow. The ridge in the contour map coincides with the slip line drawn through the corner of the opening. On the other hand, in Case 2, the interval of the contour lines is more wide, then the value of $(\varepsilon_1^p - \varepsilon_3^p)$ decreases gradually as a ripple. However, the patterns of the contour map in the region less than $5 \times 10^{-3}$ are almost the same in both cases.

Assuming that the rock mass is fractured through the slip lines when the plastic shear strain reaches its limitation, the fracture surface is considered to be generated along the ridge in the contour map of the plastic region and almost parallel to the elastoplastic interface. It is clear that

 

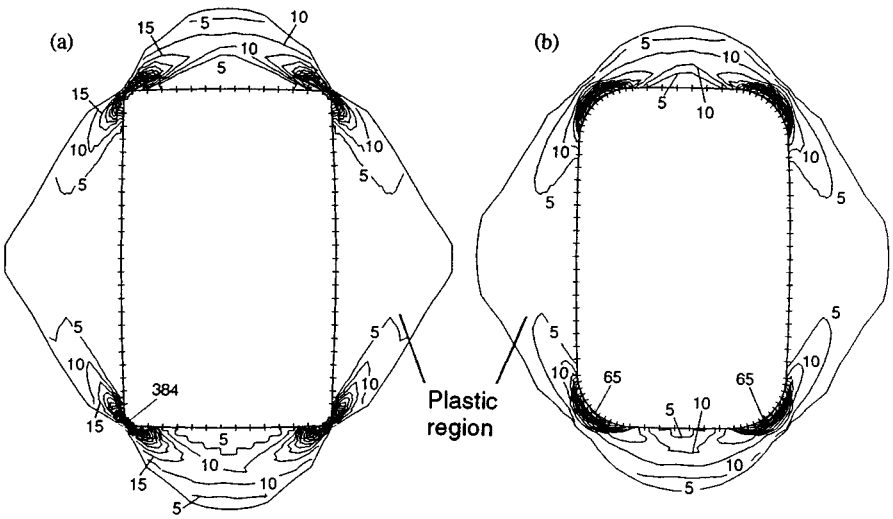


Figure 9. Contour map of the maximum plastic strain ($\varepsilon_1^p - \varepsilon_3^p$) in the plastic region in the case of using associated flow rule, dilatancy angle $\phi_N = 40^\circ$ (unit of numerals in figure is $10^{-3}$); (a) Case 1, (b) Case 2

the shape of the opening in Case 1 can be initiated by the fracture surface around the opening with greater ease than that in Case 2. If the fracture surface should be generated in both cases, the depth of the intersection of the fracture surface appeared at the centre of the sidewall in Case 1 is greater than that in Case 2.

*Horse-shoe shaped opening*

The displacement and strain field around a house-shaped opening, which is excavated in a rock mass under general biaxial initial stress state, are shown in Figure 10. The opening is 11·5 m in width and 8·5 m in height. The radii of the upper part and both sides of the floor of the opening are 5·75 and 0·05 m.

The slip lines are drawn in the plastic region in Figure 10(a). The depth of the plastic region near the point A, which is the point in the plane perpendicular to the maximum initial principal stress, is larger than that near the point B, which is in the plane parallel to the maximum initial principal stress, in the arch of the opening. Comparing the elastoplastic displacement with the elastic displacement, the former is larger than the latter. In particular, the different between them is remarkable near the point A. The latter is large near point A and small near the point B. Conversely, the former is small near the point A and large near the point B. Therefore, when the back analysis performed using the displacements in the plastic region, the direction of the maximum initial principal stress may be made a mistaken estimation as that of the minimum initial principal stress.

The contour map of the plastic shear strain is shown in Figure 10(b) with the shape of the elastoplastic interface. The concentration of the plastic shear strain exists at the corners of the opening. The ridge of the contour coincides with the slip lines drawn through the corners. This

 

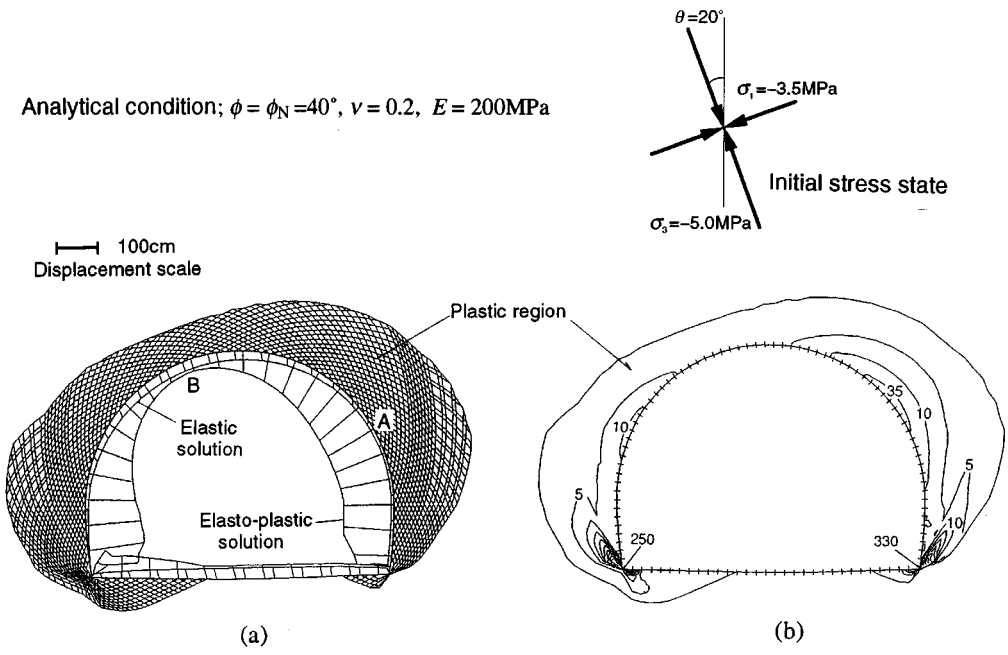


Figure 10. Solution of a horse-shoe shaped opening, which is 11.5 m in width and 8.5 m in height and the radii of the upper part and the both sides of the floor of it are 5.75 m and 0.05 m, under biaxial initial state; (a) shape and extent of the plastic region, and displacement of the opening wall, (b) contour map of the maximum plastic strain ($\varepsilon_1^p - \varepsilon_3^p$) in the plastic region (unit of numerals in figure is $10^{-3}$)

result suggests that the fracture occurs through the corners of the opening and that the fracture surface is not identified with the elastoplastic interface.

From these results, the forming smooth surface of the opening is important from the viewpoint of evading the concentration of the plastic shear strain. It is considered that the shotcreate just after blasting in tunneling might involve the effect of evading the concentration of the shear strain around the tunnel. Furthermore, it is desired that the radius of curvature at the corner is as large as possible when the opening is constructed.

## CONCLUSIONS

The coupled Boundary Element Method - Characteristics Method (BEM-CM), in which the non-associates flow rule is introduced to calculate the displacement and strain field in plastic region around underground opening, was presented.

Applying the BEM-CM to circular underground opening, it was shown that this method is one of the accurate and effective methods for solving the excavation problem of underground openings. Furthermore, analysing the strain distribution in the plastic region, it was made clear that the failure mechanism may be investigated from the distribution of the maximum plastic-shear strain. Finally, it was noted that the shotcreate just after blasting in tunnelling involve the effect of evading the concentration of the shear strain around the tunnel due to the forming of a smooth surface.

 

## APPENDIX

The Mohr–Coulomb's yield function which is expressed as follows is adopted in this analysis

$$\tau = C + \sigma \tan \phi \tag{32}$$

where $\tau$ and $\sigma$ are the shear and the normal stress, respectively, and $C$ and $\phi$ are the cohesion and the internal friction angle, respectively. Moreover, the plastic potential which is of the same type as the yield function is defined at a plastic stress state as

$$\tau = C_{\mathrm{p}} + \sigma \tan \phi_N \tag{33}$$

where $C_{\mathrm{p}}$ is a constant dependent on the plastic stress state and $\phi_N$ is the dilatancy angle. Equations (32) and (33) are rewritten in terms of the principal stresses $\sigma_1$ and $\sigma_3$ as

$$\sigma_1 = S_{\mathrm{c}} + q\sigma_3 \tag{34}$$

$$\sigma_1 = S_{\mathrm{p}} + q_N\sigma_3 \tag{35}$$

$$S_{\mathrm{c}} = 2C \tan\left(\frac{\pi}{4} + \frac{\phi}{2}\right) \tag{36}$$

$$S_{\mathrm{p}} = 2C_{\mathrm{p}} \tan\left(\frac{\pi}{4} + \frac{\phi_N}{2}\right) \tag{37}$$

$$q = \tan^2\left(\frac{\pi}{4} + \frac{\phi}{2}\right) \tag{38}$$

$$q_N = \tan^2\left(\frac{\pi}{4} + \frac{\phi_N}{2}\right) \tag{39}$$

where $S_{\mathrm{c}}$ is the uniaxial compressive strength and $S_{\mathrm{p}}$ is a constant corresponding to $C_{\mathrm{p}}$.

The condition of equilibrium in the plastic region around a circular underground opening of radius $R$ under the hydrostatic initial stress field $\sigma_0^{\infty}$ ($> S_{\mathrm{c}}/2$) is given by

$$\frac{\mathrm{d}\sigma_{\mathrm{r}}}{\mathrm{d}r} = \frac{\sigma_\theta - \sigma_r}{r} \tag{40}$$

in the pole co-ordinates. In addition, the plastic region is defined as $R^* < r < R$, where $R^*$ is the radius of the elastoplastic interface. As the yield function in the pole co-ordinates is written by

$$\sigma_\theta = S_{\mathrm{c}} + q\sigma_r \tag{41}$$

the normal stress component in the radial direction in the plastic region is obtained by

$$\sigma_r = S_{\mathrm{c}} \frac{1 - (r/R)^{q-1}}{1 - q} \tag{42}$$

On the other hand, the stress state in the elastic region ($r > R^*$) is represented by

$$\sigma_r = \sigma_0^{\infty} - \frac{(q-1)\sigma_0^{\infty} + S_{\mathrm{c}}}{q-1} \frac{R^*}{r} \tag{43}$$

$$\sigma_\theta = 2\sigma^{\infty} - \sigma_r \tag{44}$$

 

Since $\sigma_r$ continues at $r = R^*$, $R^*$ is given by

$$\left(\frac{R^*}{R}\right)^{q-1} = \frac{2\{(q-1)\sigma_0^\infty + S_c\}}{S_c(q+1)} \tag{45}$$

Equation (45) is rewritten in terms of $n = \sigma_o^\infty / S_c$ as

$$\left(\frac{R^*}{R}\right)^{q-1} = \frac{2\{(q-1)n+1\}}{q+1} \tag{46}$$

The displacement under a hydrostatic initial stress field is produced in the radius direction. Under the plane strain condition, the displacement $\xi$ in the radial direction in the elastic region is represented by

$$2G\frac{\xi}{r} = (1-v)\sigma_0^\infty + \frac{(q-1)\sigma_0^\infty + S_c}{q+1}\left(\frac{R^*}{r}\right)^2 \tag{47}$$

where $G$ is the shear modulus and $v$ is the Poisson's ratio. The first term in the above equation represents the initial displacement and the second one is the displacement due to the excavation of the circular opening.

The strain in the plastic region which is defined as the summation of the elastic strain and the plastic strain is expressed as

$$\varepsilon_r = \varepsilon_r^e + \varepsilon_r^p = \frac{\partial \xi}{\partial r} \tag{48}$$

$$\varepsilon_\theta = \varepsilon_\theta^e + \varepsilon_\theta^p = \frac{\xi}{r} \tag{49}$$

where superscripts e and p represent the elastic strain and the plastic strain, respectively. Since $\varepsilon_r^p$ and $\varepsilon_\theta^p$ are the principal strains, we can obtain the following relation:

$$\varepsilon_r^p = -q_N \varepsilon_\theta^p \tag{50}$$

Therefore, the following differential equation is obtained in terms of equations (48) and (49):

$$\frac{\partial \xi}{\partial r} + q_N \frac{\xi}{r} = q_N \varepsilon_\theta^e + \varepsilon_r^e \tag{51}$$

The strains $\varepsilon_\theta^e$ and $\varepsilon_r^e$ are given by the plastic stress state represented by equations (43) and (44) as

$$2G\varepsilon_r^e = \frac{S_c}{1-q}\{(1-2v) - (1-v-qv)(r/R)^{q-1}\} \tag{52}$$

$$2G\varepsilon_\theta^e = \frac{S_c}{1-q}\{(1-2v) - (q-v-qv)(r/R)^{q-1}\} \tag{53}$$

Consequently, we obtain the solution of equation (51) under the condition of $r = R^*$ as follows:

$$2G\frac{\xi}{r} = \frac{S_c}{1-q}\left\{(1-2v) - \frac{(1-v)(qq_N+1) - v(q+q_N)}{q+q_N}\right\}\left(\frac{r}{R}\right)^{q-1} + \frac{2(1-v)}{q+q_N}\{(q-1)\sigma_0^\infty + S_c\}\left(\frac{R^*}{r}\right)^{q+1} \tag{54}$$

 

Therefore, the displacement due to excavation is given by

$$2G\frac{\Delta\xi}{r} = 2G\frac{\xi}{r} - (1-2\nu)\sigma_0^{\infty} \tag{55}$$

## REFERENCES


1. O. C. Zienkiewicz, *The Finite Element Method*, 3rd edn, McGraw-Hill, New York, 1977.
2. T. Aoki, K. Sugawara, Y. Obara and Y. Suzuki, 'Elasto-plastic deformation of a circular opening under biaxial stress condition', *J. Mining Metall. Int. Japan*, **104,** 489–494 (1988).
3. T. Aoki and K. Sugawara, 'Elasto-plastic analysis of a single rectangular opening and parallel circular openings under biaxial stress condition', *J. Mining Metall. Int. Japan*, **105,** 511–516 (1989).
4. K. Sugawara, T. Aoki and Y. Suzuki, 'An elasto-plastic stress analysis of rock cavern under biaxial stress condition', *J. Mining Metall. Int. Japan*, **104,** 262–266 (1988).
5. K. Sugawara, T. Aoki and Y. Suzuki, 'A coupled boundary element - chracteristics method for elasto-plastic analysis of rock cavern', *Proc. Int. Symp on Rock Mechanics and Power Plant*, 1988, pp. 249–258.
6. Y. Obara, T. Aoki, H. K. Jang, T. Nakayama and K. Sugawara, 'Determination of plastic regions around underground openings by a coupled boundary element - characteristics method', *Int. J. Numer. Anal. Meth. Geomech.*, **16,** 701–716 (1992).
7. Y. Obara, T. Nakayama, K. Sugawara H. Okamura and M. Akimoto, 'Coupled boundary element - characteristics method and its application to elasto-plastic problem in rock engineering', *Proc. Int. Symp. on Assessment and Prevention of Failure Phenomena in Rock Engineering*, 1993, pp. 927–933.
8. C. A. Brebbia, *The Boundary Element Method for Engineers*, Pentrech Press, Plymouth, 1978.
9. R. Hill, *The Mathematical Theory of Plasticity*, Oxford University Press, Oxford, 1950.
10. J. C. Jeager and N. G. W. Cook, *Fundamentals of Rock Mechanics*, Chapman & Hall, London, 1968.


 